TiO_2 – SUPPORTED CATALYSTS FOR THE STEAM REFORMING OF ETHANOL

Ilenia Rossetti[1*], Josè Lasso[1], Elisabetta Finocchio[2], Gianguido Ramis[2], Valentina Nichele[3], Michela Signoretto[3], Alessandro Di Michele[4]

[1] Dip. Chimica, Università degli Studi di Milano, INSTM Unit Milano-Università and CNR-ISTM, via C. Golgi, 19, I-20133 Milano, Italy

[2] Dip. di Ingegneria Civile, Chimica e Ambientale, Università degli Studi di Genova, P.le J.F. Kennedy 1, I-16129, Genova, Italy and INSTM Unit Genova

[3] Dip. di Scienze Molecolari e Nanosistemi, Università Ca' Foscari Venezia, Calle Larga S. Marta, 2137, Venezia, Italy and INSTM Unit Venezia

[4] Dip. di Fisica - Università degli Studi di Perugia, Via Pascoli, 06123 Perugia

ABSTRACT

TiO_2 was used as support for Ni, Co and Cu to prepare catalysts for the steam reforming of ethanol, due to its known tendency to form strong metal-support interaction (SMSI) with some metals. The samples were prepared following different procedures, tuning the reducibility of the active phase and its interaction with the support. The latter parameter showed pivotal to impart suitable catalytic activity and most of all stability towards coking. Indeed, the

* Corresponding author: fax +39-02-50314300; e-mail: ilenia.rossetti@unimi.it.

insurgence of SMSI may allow to keep the active phase dispersed, improving activity and inhibiting the formation of carbon filaments over the active phase.

The comparison between different active phases (Ni, Co, Cu, 10 wt%) confirmed Ni as very active, although it has a higher tendency to form carbon filaments. This drawback may be at least partially controlled by favouring high Ni dispersion through the formation of a mixed oxide with the support. The calcination temperature, and in general the preparation procedure for the catalyst, showed of pivotal importance to establish SMSI. In particular, calcination at relatively low temperature (*i.e*. 500°C) induced initially a higher dispersion of the active phase (mean Ni crystal size 7 nm), however not accompanied by sufficient stabilisation during activity testing (mean Ni crystal size increased to 44 nm). By contrast, calcination at higher temperature (*i.e.* 800°C) favoured the instauration of a SMSI and the formation of a mixed oxide ($NiTiO_3$), which, after activation, allowed the coexistence of smaller particles, more active and resistant to deactivation and sintering, together with the more sintered ones (mean Ni crystal size 27 nm before and after activity testing). Different characterisation data (XRD, FT-IR, TPR, TEM) allowed to conclude the need of calcination at high temperature to achieve sufficient activity and resistance of the catalyst for this application.

Co and Cu proved more promising as for C balance, although their activity at low temperature was unsatisfactory, mainly due to poor activity for C-C bond cleavage.

The characterisation of the spent catalysts by XRD, TEM and Raman allowed to evidence the different types of C deposed and to check for active phase stability against sintering.

Keyworkds: Ethanol steam reforming; Nickel catalyst; Cobalt catalyst; Copper catalyst; Titania; Metal-support interaction.

1 – INTRODUCTION

Ethanol Steam Reforming (ESR) is a promising reaction to produce H_2 from a renewable and non toxic source [1-5]. It is an endothermal reaction, usually taking place around 700-800°C.

A detailed description of reaction mechanism may be found elsewhere [6]. Along with the desired steam reforming and water gas shift (WGS) reactions, some competitive pathways may occur, depending on temperature and steam/ethanol ratio. Those particularly challenging are ethanol dehydration to ethylene, precursor of coke deposition due to its polymerisation over acidic sites, the disproportion of CO through the Boudouard reaction and the decomposition of CH_4 (formed by decomposition of ethanol) at high temperature [7,8]. Therefore, in the whole temperature range some reactions leading to catalyst coking may be active. At high temperature, carbon gasification by steam may keep under control the phenomenon, particularly at high steam/ethanol ratio. Below 600°C coke may accumulate due to the coexistance of different coke forming reactions and slow gasification [9]. Nevertheless, some

catalyst formulations are active at relatively low temperature, raising the interest in operating around 500°C to limit the heat input to the reactor and to improve H_2 yield by favoring the exothermal WGS reaction. Under such operation conditions catalyst resistance to coking is very critical. Therefore, in this work we focused our attention to operation at 500°C, trying to understand the limits for applicability in such conditions and the catalyst requirements to exploit high activity [10]. Additional testing at higher temperature also allowed to further explore the reactivity of the proposed catalysts from a more applicative point of view.

Among non-noble metals, Ni demonstrated a very promising active phase due to its ability to activate the C-C bond and Co was suggested to improve the WGS activity and to operate at lower temperature [1,11-13]. Unfortunately, both Ni and Co may easily form carbon deposits in the form of filaments, especially when poorly dispersed in form of big particles [14-17].

In our previous investigations we focused on some Ni-, Co- and Cu-based catalysts evidencing the effect of catalyst formulation and of the preparation method on its performance [12,13,18]. We found that in the case of Ni the metal-support interaction plays a key role in keeping the active phase dispersed, thus avoiding extensive coking [12]. The strength of the metal support interaction also showed important for Pt-based catalysts [19]. However, also the redox properties of the catalytic system may influence activity [13].

In the present work we compared Ni, Co and Cu as active phases, supported over TiO_2. This support, which was scarcely investigated for this application, may exhibit different acidic and redox properties with respect to other supports,

such as silica or zirconia. Furthermore, it may be prepared in different crystal habits, which in principle may differently host the selected active phases and its ability to develop strong metal support interaction with some metals is well known [20-22]. The pivotal effects of the nature of the active phase and of its interaction with the support have been taken into account here to interpret the catalyst behavior.

2 – EXPERIMENTAL

2.1 – Catalyst preparation

A summary of the preparation conditions and of the main physical chemical properties of each sample is reported in Tables 1 and 2.

2.1.1 - Support synthesis in liquid phase

TiO_2 was prepared through a conventional precipitation method [23]. 20 g of $TiOSO_4$ xH_2SO_4 xH_2O (Sigma Aldrich, purity synthesis grade) were dissolved in 300 mL of distilled water at r.t., then NaOH (Carlo Erba, 9 M) or NH_3 (Riedel-de Haën, 9 M) was added dropwise until the system reached a pH of 5.5. The precipitate was aged at 60°C for 20 hours, then repeatedly washed with distilled water and finally dried overnight at 110°C.

2.1.2 – Addition of the active phase

The active phase was added to each support by incipient wetness impregnation with an aqueous solution of the metallic precursor ($Ni(NO_3)_2*6H_2O$, Sigma Aldrich, purity ≥98.5%; $Co(NO_3)_2*6H_2O$, Sigma Aldrich, puriss. p.a. ACS reagent; $Cu(NO_3)_2*3H_2O$, Sigma Aldrich, puriss. p.a.), in the proper concentration in order to obtain the desired metal loading (10 wt%). The catalyst was dried overnight at 110°C and then calcined in air at 500 or 800°C at a rate of 2°C/min for 4 hours.

Catalysts were named T_xCYM, where T refers to TiO_2, x=S or A means precipitation of TiO_2 with NaOH or NH_3, Y = 5 or 8 represents the calcination temperature at 500 or 800°C and the last symbol indicates the active phase (M=Ni, Co, Cu).

2.2 - Characterisation

Atomic absorption spectroscopy measurements were carried out on a Perkin Elmer AAnalyst instrument after dissolution of the sample.

X-ray powder diffraction (XRD) patterns were collected on a Bruker D8 Advance diffractometer equipped with a Si(Li) solid state detector (SOL-X) and a sealed tube providing Cu Kα radiation. Phase recognition was possible by comparison with literature data [24]. Rietveld analysis was carried out on some of the reduced (at 500°C or 800°C) and spent samples.

Specific surface area and pores size distribution were evaluated by N_2 adsorption-desorption isotherms at -196°C (Micromeritics, ASAP 2000 Analyser). Surface area was calculated on the basis of the BET equation [25],

whereas the pores size distribution was determined by the BJH method [26], applied to the N_2 desorption branch of the isotherm. Prior to the analysis the sample was dried overnight at 110°C and then outgassed at the same temperature for 2 hours.

The TPR technique was employed to identify different metallic species possibly present in the catalysts according to the different reduction temperatures; moreover, this technique allows to evaluate the existence of potential interactions between the active phase and the support. The catalyst was placed in a quartz reactor and heated by 10°C/min from *r.t.* to 800°C in a 5% H_2/Ar mixed gas stream flowing at 40 mL/min.

TEM images have been obtained using a Philips 208 Transmission Electron Microscope. The samples were prepared by putting one drop of an ethanol dispersion of the catalysts on a copper grid pre-coated with a Formvar film and dried in air.

FT-IR spectra have been recorded in static conditions by a Nicolet Nexus Fourier transform instrument, using conventional IR cells connected to a gas manipulation apparatus (OMNIC™ software, DTGS detector). Pressed disks of pure catalyst and support powders (~20 mg) were thermally pretreated in the IR cell by heating in vacuum at 500°C. They were heated in pure H_2 at 500°C or 450°C (600 Torr, two cycles, 30 min each) to reduce the samples, followed by an evacuation step at the same temperature. CO adsorption experiments have been performed at liquid nitrogen temperature recording spectra following outgassing up to r.t.. Pivalonitrile (PN, Aldrich, pur. 98%) adsorption

experiments have been performed over the reduced samples at r.t. and following outgassing at increasing temperature.

Skeletal spectra have been recorded in air, after dilution of the catalyst powder with KBr (Aldrich, FT-IR grade) (0.1% w/w). Far-IR spectra (400-50 cm^{-1}) have been recorded using pure catalyst powder deposited on polyethylene ('solid substrate' beam splitter).

UV-Vis, NIR spectra of catalyst pure powders have been recorded in air, by a Jasco 570V instrument equipped with a DR cell.

Micro-Raman sampling was made by an OLYMPUS microscope (model BX40) connected to an ISA Jobin–Yvon model TRIAX320 single monochromator, with a resolution of 1 cm_1. The source of excitation was a Melles Griot 25LHP925 He-Ne laser that was used in single line excitation mode at l=632.8 nm. The power focused on the samples was always less than 2 mW. The scattered Raman photons were detected by a liquid-nitrogen cooled charge coupled device (CCD, Jobin Yvon mod. Spectrum One).

2.3 – Ethanol steam reforming (ESR)

Details on the equipment for activity testing may be found elsewhere [12]. Briefly, the catalysts were pressed, ground and sieved into 0.15-0.25 mm particles and *ca*. 0.5 g were then loaded into the reactor after dilution 1:3 (vol/vol) with SiC of the same particle size. Catalyst activation was accomplished by feeding 50 cm^3/min of a 20% H_2/N_2 gas mixture, while heating

by 10°C/min up to 500°C for 1 h for the samples calcined at 500°C. By contrast, samples calcined at 800°C were heated up to 800°C then kept for 1h.

During activity testing 0.017 cm^3/min of a 3:1 (mol/mol) H_2O:CH_3CH_2OH liquid mixture were fed to the reactor by means of a Hitachi, mod. L7100, HPLC pump, added with 56 cm^3/min of N_2, used as internal standard, and 174 cm^3/min of He. Such dilution of the feed stream was calibrated so to keep the reactants mixture in the vapour phase even at zero conversion at the reactor outlet.

The activity tests were carried out at atmospheric pressure, GHSV = 1750 h^{-1} (referred to the ethanol + water gaseous mixture) at 500°C. Samples calcined at 800°C were also tested at 625 and 750°C.

The analysis of the out-flowing gas was carried out by GC analysis. Repeated analyses of the effluent gas were carried out every hour and the whole duration of every test at each temperature was *ca*. 8 h. The raw data, expressed as mol/min of each species outflowing from the reactor, averaged after 4-8 h-on-stream, have been elaborated as better detailed in [12].

3 - RESULTS AND DISCUSSION

According to our previous investigations, Ni usually showed very active, selective and stable when tested at temperature higher than 600°C. On the contrary, it proved sufficiently resistant to coking when operating at 500°C provided that very small particle size was achieved during preparation and kept

stable by establishing a sufficiently strong interaction with the support [10,12,13,18,27]. TiO_2 was reported as a support able to develop a strong metal support interaction (SMSI) with some metals [20-22], therefore it was chosen in this work as support for Ni at first [27]. Comparative samples containing Co and Cu as active phases were also considered.

The SMSI effect has been studied in the past [20], starting from the evidence that the chemisorption properties of supported noble metals were dramatically altered by interaction with a TiO_2 surface. The results were markedly different depending on the calcination temperature [20,22]. The possibility of metal surface coverage by titanium oxide was one of the evidences in some cases [22] and additionally an intermetallic bonding was hypothesised, so strong to modify the chemisorption properties of the metal [20]. It was found that the mobility of Ti ions was sufficient to allow the coverage of portions of the metal and this, as well as the formation of intermetallic compounds, was more likely in cases of partial reduction of TiO_2 (TiO_x) [21]. As a matter of fact, such interaction may act in different ways, changing the electronic state of the active metal, modifying its dispersion, or even creating some special active sites at the interface between the metal and the support. The interaction of metal/TiO_x systems with CO and H_2 has been particularly deepened, stressing that perimetral sites may exhibit particular activity for CO dissociation [21,28], which in the present case may favour coke formation. Additionally, a spillover effect has been often evidenced for H_2 further favouring titania surface reduction.

3.1 – Ni-based catalysts

3.1.1 – Activity testing

Low temperature tests for ethanol SR have been carried out at 500°C on each catalyst and the results are summarised in Table 3.

The major challenge for Ni-based samples is usually ascribed to coking, often due to the formation of carbon filaments over the active phase at relatively low temperature. This phenomenon is sometimes correlated also to catalyst deactivation and appearance of by-products. Indeed, operation at 500°C showed C balance often much lower than 100% (C balance for blank test closing at *ca.* 91%, with C deposition over the quartz beads filling the reactor), as evidenced in Table 3. H_2 productivity at 500°C seemed firmly dependent on the calcination and on activation temperature of the catalyst. For instance, samples T_SC5Ni and T_AC5Ni, calcined at 500°C, performed much worse than the parent samples, T_AC8Ni and T_SC8Ni, calcined at 800°C. Only limited ethanol conversion was attained with the former samples and selectivity to acetaldehyde and CO_2, only. Catalyst T_SC5Ni in particular showed full ethanol conversion during the first minutes on-stream, but it rapidly deactivated leading to the steady state activity values reported in Table 3. In addition, the carbon balance was largely unsatisfactory for the whole test. A bit higher stability was shown by sample T_SC5Ni, whose support was prepared by precipitation from NaOH, than T_AC5Ni, prepared by adding NH_3 (Table 1). No significant difference of catalyst performance was observed by increasing their activation temperature to 700°C.

By contrast, when calcining and activating the samples at 800°C, a completely different behaviour was observed. Sample T_AC8Ni showed full ethanol

conversion at the beginning of the test, with the highest H_2 productivity. The results were similar to T_SC8Ni, which additionally exhibited a bit better carbon balance (Fig. 1*a*). However, after *ca*. 4 h-on-stream, sample T_AC8Ni started deactivating, with simultaneous increase of selectivity to acetaldehyde (Fig. 1*b*). On the contrary, sample T_SC8Ni was stable for the whole duration of the test, with negligible selectivity to acetaldehyde, confirming the better stability of samples prepared from TiO_2 precipitated by NaOH (Fig. 1*c*).

Both the samples calcined at 800°C were also tested at 625 and 750°C, under more industrially relevant conditions. Full C balance was achieved for both samples. This indicates negligible C accumulation over these samples at higher temperature and the effective gasification of most C accumulated during testing at lower temperature. Indeed, 120% C balance was observed during testing at 625°C for the first h-on-stream, then stabilised around 100%. Stable full conversion of ethanol and products distribution were also observed. H_2 productivity also increased at 750°C to *ca*. 1.5 and 1.2 mol/min kg_{cat} for samples T_AC8Ni and T_SC8Ni, respectively.

3.1.2 – Catalysts characterisation

Samples T_SC5Ni and T_AC5Ni exposed the same surface area (*ca*. 100 m^2/g), whereas T_AC8Ni and T_SC8Ni, calcined at 800°C, had very low surface area. Ni crystal size, determined by Rietveld analysis, is reported in Table 1 for the samples reduced at 500 or 800°C (according to the calcination temperature). Due to the higher calcination temperature, bigger Ni crystal size was in average obtained for samples calcined (and reduced) at the highest temperature.

However, the analysis was repeated after activity testing on samples T_SC5Ni and T_SC8Ni showing that, on the contrary, sintering occurred for the sample calcined at 500°C, but not for the one calcined at higher temperature, Ni being more strongly stabilised by a stronger interaction with the support.

Ni crystal size is very critical as for the formation of carbon filaments. Indeed, it is reported in the literature that the formation of carbon filaments over smaller Ni particles is inhibited with respect to bigger ones [14-17]. However, we previously correlated catalyst performance also to the stabilisation of the Ni active phase by the support through formation of a strong metal-support interaction [12,13,18], which would help in keeping dispersed the active phase during the reaction, thus limiting coke deposition. A simple analytical tool to investigate such parameter is TPR analysis, which identifies the reduction temperature of the active phase. The lowest the metal ion reducibility, the highest its stability. This is usually attributed to higher metal dispersion and to a stronger metal/support interaction.

The TPR patterns of all these samples are reported in Fig. 2 and H_2 uptake per mol of NiO is reported in Table 1. H_2 consumption was much higher for samples calcined at 500°C than at 800°C. This likely indicates some spillover of H_2 towards the support with its possible partial reduction. This is most likely for the anatase structure, present in the samples calcined at 500°C, than for the rutile one, mostly constituting the samples calcined at 800°C (*vide infra*).

Furthermore, it is clearly visible from Fig. 2 that the T_SC5Ni and T_AC5Ni samples were characterised by much higher reducibility than T_AC8Ni and T_SC8Ni and showed worse activity. It seems that a higher reducibility (*i.e.* larger

Ni particles with weaker interaction with the support) is correlated with faster deactivation and poor activity. By contrast, with increasing the calcination temperature during preparation one may achieve more stable Ni particles due to stronger interaction with the support [29].

This trend is confirmed by the present data. Indeed, sample T_SC5Ni, initially exhibiting very small Ni crystallites, also showed higher reducibility (*i.e*. weaker interaction strength with the support [22]). As a consequence of poor metal stabilisation of the support some sintering occurred upon activity testing, at the contrary of sample T_SC8Ni, much less reducible, which did not sinter significantly during activity measurements (see also TEM of spent catalysts).

In the case of Ni supported over titania, the high temperature of calcination may also induce the formation of mixed oxides, as confirmed by XRD (*vide infra*), which may further help the segregation of the active phase [29-31].

We can conclude that the reducibility trend may be correlated to catalyst performance. The lowest the catalyst reducibility (high Ni stabilisation by the support), the better the catalytic performance and catalyst stability.

The most recent reaction mechanisms highlight the role of the support in adsorption and activation of ethanol and water, which subsequently react on the active phase. Thus, the role of metal-support boundary surface assumes higher importance, further supporting the positive effect of high metal dispersion and SMSI on catalytic performance and on products distribution [32-34].

In order to better support this point, we activated the samples mimicking the activation conditions and we collected TEM micrographs (Fig. 3). By comparing samples T_SC5Ni and T_SC8Ni one may see that the former, activated at 500°C,

was constituted by very homogeneous TiO_2 nanoparticles, *ca*. 20-30 nm in size. Darker spots represent Ni particles, randomly and non-homogeneously distributed over the support, with variable size (5-10 nm), in accordance with XRD data. By contrast, sample T_SC8Ni, activated at 800°C, showed a much more sintered support, over which Ni particle size of variable size coexist. Indeed, bigger metal particles 10-20 nm are accompanied by very homogeneous and smaller particles which size was *ca*. 1-2 nm.

Based on this evidence and on TPR pattern we can confirm that calcination at higher temperature favoured the presence of part of the metal in smaller particles thanks to a stronger interaction with the support. Indeed, even though sample T_SC5Ni was calcined at lower temperature than T_SC8Ni, the latter showed the persistence of a fraction of smaller particles after activation. The latter in principle should be more stable towards the formation of carbon nanotubes than the bigger ones [10].

Furthermore, by comparing the diffractograms of the titania supported samples with literature data, one may conclude that sample T_SC5Ni was mainly constituted by anatase, with *ca*. 10wt% of brookite, whereas sample T_AC5Ni fully consisted of anatase. Consistently, the FT-IR skeletal spectra of both T_SC5Ni and T_AC5Ni samples show the broad absorption centred at 470 cm^{-1}, characterising the titania anatase phase (not reported).

The quantitative XRD analyses of both samples calcined at 500°C underestimated the Ni amount (*ca*. 4 wt%). Considering the existence of interactions between NiO particles and the support, as revealed by TPR measurement, it is possible to suppose that the metal partially entered in the

anatase structure of the support, leading to small and well dispersed aisles of mixed oxide, undetectable by this technique, as already evidenced elsewhere [23,35-37]. The latter became evident after calcination at 800°C. Indeed, both the samples T_AC8Ni and T_SC8Ni were constituted by rutile, plus *ca*. 15-17 wt% of ilmenite ($NiTiO_3$), as confirmed by the TPR profiles (*vide supra*). Features typical of the $NiTiO_3$ and rutile phases also appeared in the skeletal IR spectra (not reported).

These results also indicated that NiO species supported on anatase were by far more reducible than those supported on rutile and, of course, than the mixed oxide phase. However, the former samples revealed much less stable and active during activity testing. Therefore, the stabilising effect of the calcination at higher temperature may be ascribed to the formation of a mixed oxide, which keeps at least a fraction of the metal well dispersed in spite of the high activation temperature. This leads to very fine Ni particles after activation (Fig. 3*b-d*), which may be more active. Indeed, the Ni crystal size of the spent catalysts T_SC5Ni and T_SC8Ni is reported in Table 1. It is evident that, even if initially more dispersed, Ni tends to sinter when the sample is calcined at 500°C (*i.e.* more reducible and thus less strongly interacting with the anatase support). By contrast, no evident modification of crystal size was observed for the sample calcined at 800°C, much less reducible, more strongly interacting with the rutile support (and more active and stable towards deactivation at least for the testing time).

FT-IR spectra of the T_SC5Ni and T_AC5Ni samples after heating at 500°C in vacuum have a very small transmittance window and showed a high noise. The subtraction spectra recorded after CO adsorption showed only weak and broad

bands between 2200 and 2180 cm^{-1}, due to CO coordinated over surface Ti ions (spectra not reported). Apparently, no carbonyl complexes over metallic Ni species could be detected. The same samples following reduction in H_2 did not allow any IR analysis due to the very low transmittance, if any. This result further support the hypothesis of Ni incorporation into the anatase lattice or a surface reconstruction by titania.

FT-IR spectra of surface species arising from low temperature CO adsorption over the samples T_SC8Ni [18] and T_AC8Ni are reported in Fig. 4. Low temperature CO adsorption gave rise to a series of bands in the C-O spectral region due to: *i*) CO interacting with OH groups and CO adsorbed over Ni ions (this band completely disappeared following outgassing at low temperature); *ii*) (di)-carbonyl species stable at low temperature adsorbed over a dispersed Ni^+ fraction; iii) (poly)-carbonyl species on Ni^0 highly dispersed phase; *iv*) CO adsorbed on larger Ni^0 particles exposing flat surfaces. No bands due to CO coordinated over exposed Ti centres could be detected. This observation can be explained by the collapse of surface area in these samples and also by to the formation of a titanate phase, as pointed out by XRD results. The present results also confirm the coexistence of larger and smaller Ni particles after activation.

CO adsorption over T_AC8Ni catalyst, whose corresponding spectra are reported in the same Figure, allowed the detection of weak and very noisy bands in the carbonyl region, likely due to the very low surface area of this sample. However, it was possible to roughly detect the same features discussed for the T_SC8Ni sample. Thus, for both samples, regardless the preparation procedure, a quite heterogeneous population of Ni species is detected, formed by highly dispersed

Ni metal particles strongly interacting with the surface, Ni clusters, Ni ionic species (likely NiO, but also titanate species, corresponding to ions having different redox properties). This effect is in agreement with the TPR data, indicating for these samples the main reduction peaks at temperatures above 600°C, and with TEM micrographs evidencing the formation of Ni particles with variable size.

FT-IR analysis after treatment of T_SC5Ni and T_AC5Ni samples at 500°C did not show almost any interaction with the selected probe molecules. By looking at TPR patterns one may notice that the activation treatment under reducing atmosphere at 500°C should be sufficient to reduce NiO to Ni for both samples. However, in order to check this point a reactivation of the sample at 700°C was also attempted, aiming both at fully reduce the metal and to partially sinter it. No change of activity was attained. One hypothesis that may justify both the absence of IR absorbance and of catalytic activity is the surface reconstruction of titania, possibly covering the active phase as above discussed. This phenomenon was active for the samples calcined at very low temperature due to the high metal dispersion and the low interaction strength between the metal and the support (anatase), also evidenced by the high metal reducibility. Another possible explanation was advanced for some La-supported Ni samples, which showed inactive at low temperature due to NiO formation through oxidation by water, which led to inactive samples at low temperature [38].

By combining all these data, we may conclude that Ni/TiO_2 catalysts may exhibit satisfactory activity for the present reaction at 500°C only if calcined at high temperature in order to achieve a strong metal-support interaction, which keeps Ni more stably anchored to the support due to a SMSI effect and, thanks

to the formation of a mixed oxide allows the formation of very small Ni particles upon activation.

However, it should be remarked that satisfactory C balance, ruling out any possible catalyst deactivation by coking, may be achieved only by testing at higher temperature (*e.g*. 625°C). Indeed, even if the high temperature calcination followed by reduction leads to very small (1-2 nm) Ni particles, which are less prone to C deposition, they coexist with largeer ones, which are very likely the reason for the fast C deposition over these catalysts at 500°C.

3.2 - Co- and Cu-based catalysts

3.2.1 – Activity testing

The key point to be solved to improve the performance of the above reported Ni-based catalyst is the still unsatisfactory carbon balance, partly due to the support acidity, partly to the metal, which is prone to the formation of C filaments, especially when particle size is big. We also discussed the importance of establishing a SMSI, depending on the metal and support cation nature. Therefore, keeping the same TiO_2 support and preparation methods, we compared to the previous Ni samples some Co- and Cu-based catalysts. The latter metals, supported over TiO_2 and SiO_2, in order to compare the active phase over a support with different electrical conductivity, were already tested for the SR of ethanol at high temperature [13]. The results of activity testing at 500°C are reported in Table 4.

Co- and Cu-based catalysts, in spite of the usually better carbon balance, proved in general less active than Ni-based ones when tested at 500°C. Furthermore, their activity for the WGS reaction was very limited, contributing only marginally to decrease the CO/CO_2 ratio, and their selectivity was mainly to acetaldehyde.

Co-based catalysts gave rise to unsatisfactory results as for ethanol conversion and H_2 productivity when tested at 500°C. Sample T_AC5Co was selective almost only to acetaldehyde and CO_2, with negligible H_2 productivity and decreasing ethanol conversion (starting from *ca.* 55% down to 32%). A bit better behaviour was manifested by sample T_SC5Co, which fully converted ethanol at the beginning of the test, though it progressively deactivated down to 50% conversion. Interestingly, selectivity to acetaldehyde increased from 20 to 57%, whereas that to methane remained constantly around 3.5%. This behaviour deserves further deepening because the deactivation of the active phase, irrespectively if Ni or Co, was always accompanied by increasing selectivity to acetaldehyde and increasing C balance.

The performance of the present Co-based samples is less promising than that reported by other research groups for low-temperature steam reforming [39,40]. The selectivity for these catalysts seems linked with oxidation state, favouring or not the formation of acetate ions, considered key intermediates during ESR. The selectivity toward hydrogen and carbon dioxide was attributed to a less reduced state of cobalt, while acetates decompose to methane and CO_x species over more (or completely) reduced surfaces [41,42].

Furthermore, Co itself may form carbon filaments and it suffers deactivation by sintering and surface oxidation [39]. In addition, its lower C-C cleavage ability with respect to Ni retains some ethylene in contact with the catalyst, which is a good precursor for filaments formation [39].

For the set of samples containing Cu, catalyst T_AC5Cu surprisingly overperformed all the others as for ethanol conversion. However, the C balance was progressively decreasing with time-on-stream, preventing its proposal as promising sample. H_2 productivity was also limited by the non-negligible selectivity to by-products, such as acetaldehyde (S_{CH3CHO} = 17%), ethylene (S_{CH2CH2} = 7%) and methane (S_{CH4} = 7%). This confirms the inability of Cu to breakup efficiently the C-C bond, especially at low temperature [13,43]. The parent sample T_SC5Cu performed even worse, exhibiting a decreasing ethanol conversion to *ca.* 14% and selectivity to acetaldehyde and CO_2 only.

Cu has been indeed discussed as a promising active phase for methanol steam reforming. However, its poor C-C bond cleavage and relatively easy sintering makes it less attractive for ethanol reforming. Nevertheless, some bimetallic Ni-Cu formulations proved interesting, the Ni phase being responsible for most of the hydrogen production, while the Cu phase decreased CO production and coke deposition [41].

C balance was in general much higher for the present Co- and Cu-containing samples than for the Ni-based ones. Recalling the results of the blank test carried out at 500°C (*ca.* 91%), one can conclude that for most of these samples there is limited additional coking on the catalyst due to the active phase (*vide infra*). Some contribution of acidity to coking may be hypothesized

for TiO_2 support, due to the presence of medium strength Lewis acid sites, but the comparison of these results with what achieved with the Ni-based samples, allows to ascribe mainly to Ni particles the promotion of coking under these operating conditions.

For both Co and Cu active phases, the main reaction path seems dehydrogenation of ethanol, as stated also elsewhere [44]. Finally, in spite of the lower activity, both metals were in general more able than Ni to promote the WGS reaction, as testified by the lower CO/CO_2 ratio in the product distribution even reaching the equilibrium value in some cases (equilibrium CO/CO_2 ratio *ca*. 0.43 at 500°C).

3.2.2 – Catalysts characterisation

The specific surface area of the Co- and Cu-containing samples was around 50 m^2/g for the samples prepared by precipitation from NaOH, 70-80 m^2/g for the samples precipitated by NH_3 (Table 2). The TPR patterns of samples T_AC5Co and T_SC5Co (Fig. 2) showed two main peaks between 400 and 700°C, which may refer to the reduction of Co_3O_4 to CoO and of the latter to Co [45]. Sample T_AC5Co, prepared by precipitation with NH_3 was characterised by a higher concentration of reducible species than T_SC5Co, which mostly reduced above 600°C.

It is worth mentioning that a debate is active on the role of metallic *vs.* oxidised Co species as active phase [46]. The deepening of this subject is out of the scope of this manuscript. However, a bit worse performance has been evidenced here with the most reducible T_AC5Co than with T_SC5Co. Based on

TPR profiles one may argue that a bit higher concentration of metallic Co is present with the former after activation at 500°C, whereas in the latter Co should be mainly present as Co^{2+}.

The TPR patterns of Cu samples supported over TiO_2 showed three peaks (Fig. 2), to be ascribed to different reduction steps of species much or less strongly interacting with the support or dispersed on it [47]. Also in this case the Cu species supported over the TiO_2 sample precipitated from NaOH (sample T_SC5Cu) proved less reducible, *i.e*. more strongly interacting with the support.

XRD analysis evidenced the presence of anatase as the only TiO_2 phase in the case of both samples T_AC5Co and T_AC5Cu, precipitated with NH_3, while a minor brookite phase was present in both samples precipitated from NaOH (19.4 and 9.3% for catalysts T_SC5Co and T_SC5Cu, respectively). This confirms the higher reducibility of the active phase when supported over anatase, likely due to a lower dispersion and/or lower interaction strength with the support, as in the case of Ni-based catalysts (*vide supra*).

Also in this case Rietveld analysis strongly underestimated the amount of active phase, confirming the hypothesis of a surface reconstruction of TiO_2 partially covering the active phase, or the formation of very dispersed mixed oxide phases unidentifiable by this technique.

The skeletal IR spectra of the Co-based samples point out the formation of a main anatase TiO_2 phase (spectra not reported) in agreement with XRD data. As for the T_SC5Co sample we can clearly notice additional sharp components at 656 and 557 and a shoulder at 458 cm^{-1}, superimposed to the main absorption, detected also in the spectrum of sample T_AC5Co, although weaker. These

bands are due to Cobalt-Oxygen vibrational modes of cobalt oxide species, likely Co_3O_4.

On both T_SC5Co and T_AC5Co samples, the formation of massive Co_3O_4 together with CoO_x clusters has also been confirmed by our Uv-Vis. NIR analyses in Diffuse Reflectance mode. Moreover, the comparison among UV-Vis data suggests that the T_SC5Co sample is dominated by absorption of divalent cobalt, while the spectrum of the T_AC5Co is dominated by a low frequency component which could be assigned to trivalent cobalt.

This is perfectly matching with TPR data which show a much bigger reduction pattern at higher temperature for sample T_SC5Co, indeed corresponding to the prevalent reduction of CoO. However, FT-IR data point out the presence of massive cobalt oxide mainly in sample T_SC5Co, supporting the bigger crystal size reported in Table 2 for such sample and TEM analysis of the spent catalysts (*vide infra*). Therefore, a higher reducibility in the present case is not related to higher dispersion of the metal and stronger interaction with the support, but to its lower oxidation state.

All the samples analysed have been reduced at 550°C in H_2 before low temperature CO adsorption. The reduction of the samples T_SC5Co and T_AC5Co leads to FT-IR spectra showing almost zero transmittance in the mid IR region (spectra not reported), possibly due to the active phase coverage by surface reconstruction of TiO_2 and/or a diffuse absorption of the IR radiation due to the reduction of titania support. A similar behaviour was observed for Ni-based catalysts and may help explaining with the same reasons the poor activity of these samples.

FT-IR skeletal spectra of samples T_AC5Cu and T_SC5Cu do not evidence peaks other than those assigned to the lattice vibrational modes of the oxide support (spectra not reported). Possibly the presence of copper species in the form of CuO_x charcterized by bands around 600 cm^{-1} [48], is masked by the strong anatase bands.

CO adsorption over sample T_SC5Cu reduced in H_2 at 500°C results in the spectra reported in Fig. 5 (top). At the lowest temperatures two main bands are detected at 2150 and 2090 cm^{-1}, both of them quite complex. The former is assigned to CO interacting with OH groups, whereas a shoulder at 2170 cm^{-1} is due to exposed Ti ions form the support. The complexity of the 2090 cm^{-1} band and its thermal behaviour deserve some discussion. Over alumina supported Cu catalyst, Escribano et al. assigned a strong band at 2115 cm^{-1} to carbonyls on copper ions or copper zerovalent clusters ("2D raft") and another component centred at 2100 cm^{-1} and tailing towards lower frequencies to terminal carbonyls on copper zerovalent particles [49]. Also Boccuzzi et al. assigned a complex band around 2100 cm^{-1} to CO coordinated over Cu metal particles, whereas features at lower frequencies are assigned to larger (and structured) metal particles, exposing different facets [50]. In our spectra the band is centred at 2090 cm^{-1}, showing a shoulder around 2085 cm^{-1}, and the position and thermal behaviour of these bands allow their assignation to Cu clusters and more structured Cu metal particles exposing mainly (110) facets. CO adsorption over the T_AC5Cu sample led to very similar results (Fig. 5, bottom). The high frequency shoulder at 2170 cm^{-1} was assigned to CO coordinated over exposed Ti ions. The band at 2149 cm^{-1} is due to CO H-bound to hydroxyl groups of the support. The band at 2102 cm^{-1}, with a shoulder at 2090 cm^{-1} and tailing

towards lower frequencies, is due to CO coordinated over Cu metal clusters and particles. Residual Cu ions are likely still present and lead to CO oxidation to CO_2, detected as a complex band at 2350 cm^{-1}.

The comparison of these two series of spectra evidenced very similar features for CO adsorbed over T_AC5Cu and T_SC5Cu samples, corresponding to the detection of highly reducible supported Cu ions, whose reduction lead to the formation of copper particles and metal clusters strongly interacting with the oxide support, in perfect agreement with the TPR pattern. However, the lower frequencies detected for the carbonyl bands over the T_SC5Cu samples point out the formation of metal particles electron richer, if compared to sample T_AC5Cu. This may help explaining the worse catalytic performance of sample T_SC5Cu.

Therefore, when the catalysts are calcined at low temperature, surface reconstruction and coverage of the metal sites by titania was achieved for Ni and Co, preventing the obtainment of satisfactory activity data, but not on Cu. The latter however is poorly active for C-C bond cleavage excluding any significant performance at low temperature.

3.3 – Characterisation of the spent catalysts

Some of the spent samples have been characterised by TEM and XRD.

As above discussed, the establishment of SMSI allowed to increase the resistance to sintering of the active phase. Indeed, an increase of the Ni particle size after activation and use has been evidenced for sample T_SC5Ni by XRD (Table 1). Furthermore, TEM data showed bigger and irregular Ni particle size

for that sample (Fig. 6*a*) with respect to T_SC8Ni (Fig. 6*b*), on whose surface a fraction of very small particles still persisted in spite of the much higher calcination and activation temperatures.

The micrographs of spent samples T_AC5Co and T_SC5Co are reported in Fig. 6*c*-*e*. Uniform and slightly sintered Co particles are observed for the former sample, whereas markedly not uniform and more sintered partiles are observed for the latter. This further confirms that the lowest reducibility of sample T_SC5Co was due to the lower oxidation state and not necessarily index of a stronger interaction with the support. In addition, the formation of nanotubes was evident for T_SC5Co, especially in connection with the largest particles. The formation of nanotubes and similar carbon deposits is correlated with the progressively decreasing acrivity and increasing selectivity to acetaldehyde, as already observed for other catalytic systems [10]. By contrast, no evidence of C nanotubes was observed for sample T_AC5Co, either due to the more uniform and smaller Co particle size, or, more likely, to the very low activity, which leads predominantly to acetaldehyde thus preventing the formation of possible carbide precursors, as in the case of samples T_AC5Ni and T_SC5Ni. Over the latter only exhibited the formation of ordered layers overing large part of the active surface (Fig. 6*a*). Some nanotubes were also observed for samples T_AC8Ni (in higher concentration) and T_SC8Ni (a few). This is consistent with a lower uniformity of Ni particle size observed for the former, in agreement with the higher reducibility, than for the latter.

Some coking was also observed on both the Cu-containing samples, although not in the form of nanotubes but as graphitic or amorphous layers, as exemplified in Fig. 6*f*.

The possible coexistence of ordered nanotubes and carbonaceous layers has been also evidenced by Raman spectra collected on the spent samples, which showed the typical D and G bands of graphite in different proportions. In Fig. 7 we reported the normalized Raman spectra of some spent samples. It is possible to observe two bands at *ca*. 1340 cm^{-1} (D band) and *ca.* 1600 cm^{-1} (G band). The intensity ratio between such bands is commonly used to measure imperfection in highly crystalline graphite material. A higher content of CNTs inhibits an ordered graphite crystallite growth and as a result, the intensity ratio between the D ang G bands increases [51].

By the analysis of spectra it is possible to observe that samples T_AC8Ni, T_SC8Ni and T_SC5Co show a higher intensity ratio I_D / I_G than other samples. This confirmeded that in the former samples CNTs are present, as demonstrated by TEM analysis.

To conclude, the low C balance comes from a combination of C forming reactions, some leading to the formation of C layers over catalyst surface. When the active phase is particularly active, at least for the first h-on stream, as in the case of T_AC8Ni, T_SC8Ni and T_SC5Co, C may also accumulate over tha active phase in forms of nanotubes. Possibly, this effect may be enhanced by the SMSI effect, which favors the formation of perimetral sites active for CO cleavage [21], which may promote the Bouduard reaction.

4 - CONCLUSIONS

TiO_2 was explored as possible support for Ni-, Co- and Cu-based catalysts for the steam reforming of ethanol, due to the documented possibility to establish a strong metal support interaction with some active phases. Because of possible accumulation of carbon deposits around 500°C, due to both support acidity and the tendency of some active phases to form filaments, the catalytic activity was explored at 500°C, focusing not only on ethanol conversion and H_2 productivity, but mostly on C balance as an index of possible coke deposition over the catalyst. Coking depends on support acidity, but in such a case it is expected that the most acidic sites are rapidly covered by carbon and ruled out. Another important aspect is the formation of carbon nanotubes over the active phase, which is usually limited when the metal particle size is small. Therefore, the development of a strong metal support interaction may help in keeping the metal dispersed and more stable during the reaction.

Ni confirmed the most active metal for this reaction, within those here investigated, but many concerns rely on its coking activity. The comparison between the active phases confirm the role of Ni on carbon accumulation over the catalyst, with a more limited contribution of support acidity.

Higher resistance to coking may be achieved when Ni more strongly interacts with the support, *i.e*. calcining at 800°C, which may lead to the stabilisation of the active phase under the reaction conditions, inhibiting sintering during activity testing. One possibility is the formation of a mixed oxide, which allows the obtainment of very small metal particles after reduction at high temperature, although coexisting with bigger ones. When calcining at low temperature, the use of this support may be detrimental due to surface reconstruction and possible coverage of the active phase by the support itself, leading to practically

inactive catalysts. This may also be ascribed to a different solubility and reducibility of Ni supported over anatase or rutile.

Therefore, the promotion of strong metal support interaction, achievable by calcination at high temperature, is important to maintain sufficient activity of the catalyst at low temperature.

On the contrary, Co and Cu did not prove sufficiently active at such low temperature, in spite of a generally better C balance and lower deactivation by coking.

ACKNOWLEDGEMENTS

The authors are indebted with Regione Lombardia and the Consortium for Material Science and Technology (INSTM) for financial support. The valuable help of the PhD student Cesare Biffi and of the MoS graduating student Mauro Castellana is gratefully acknowledged. The authors are indebted to Prof. Giuseppe Cruciani for XRD analyses and their elaboration. The characterisation was partly supported by H2FC European Infrastructure Project (Integrating European Infrastructure to support science and development of Hydrogen and Fuel Cell Technologies towards European Strategy for Sustainable Competitive and Secure Energy), project reference 284522.

REFERENCES

1. M. Ni, D.Y.C. Leung, M.K.H. Leung, Int. J. Hydrogen Energy, 32 (2007) 3238-3247.

2. V. A. Kirillov, V. D. Meshcheryakov, V. A. Sobyanin, V. D. Belyaev, Yu. I. Amosov, N. A. Kuzin, A. S. Bobrin, Theor. Found. Chem Eng., 42 (2008) 1-11.

3. L.E. Arteaga, L.M. Peralta, V. Kafarov, Y.; Casas, E. Gonzales, Chem. Eng. J., 136 (2008) 256-266.

4. V.A. de la Peña O'Shea, R. Nafria, P. Ramìrez de la Piscina, N. Homs, Int. J. Hydrogen Energy, 33 (2008) 3601-3606.

5. S.M. de Lima, I.O. da Cruz, G. Jacobs, B.H. Davis, L.V. Mattos, F.B. Noronha, J. Catal., 257 (2008) 356-368.

6. A.N. Fatsikostas, X.E. Verykios, J. Catal., 225 (2004) 439-452.

7. F. Díaz Alvarado, F. Gracia, Chem. Eng. J., 165 (2010) 649-657.

8. Y. Chen, Z. Shao, N. Xu, Energy & Fuels, 22 (2008) 1873-1879.

9. L.J.I. Coleman, W. Epling, R.R. Hudgins, E. Croiset, Appl. Catal. A: Gen., 363 (2009) 52-63.

10. I. Rossetti, J. Lasso, E. Finocchio, G. Ramis, V. Nichele, M. Signoretto, A. Di Michele, Appl. Catal. B: Environmental, 150-151 (2014) 257-267.

11. A. Casanovas, M. Saint-Gerons, F. Griffon, J. Llorca, Int. J. Hydrogen Energy, 33 (2008) 1827-1833.

12. I. Rossetti, C. Biffi, C.L. Bianchi, V. Nichele, M. Signoretto, F. Menegazzo, E. Finocchio, G. Ramis, A. Di Michele, Appl. Catal. B: Environmental, 117-118 (2012) 384-396.

13. E. Finocchio, I. Rossetti, G. Ramis, Int. J. Hydrogen Energy, 38 (2013) 3213-3225.

14. G. Centi, S. Perathoner, Catal. Today, 148 (2009) 191-205.

15. V. M. Gonzalez-De la Cruz, J.P. Holagado, R. Pereniguez, A. Caballero, J. Catal., 257 (2008) 307-314.

16. K.O. Christensen, D. Chen, R. Lodeng, A. Holmen, Appl. Cat. A: Gen., 314 (2006) 9-22.

17. D. Chen, K.O. Christensen, E. Ochoa-Fernandez, Z. Yu, B. Totdal, N. Latorre, A. Monzón, A. Holmen, J. Catal., 229 (2005) 82-96.

18. I. Rossetti, A. Gallo, V. Dal Santo, C.L. Bianchi, V. Nichele, M. Signoretto, E. Finocchio, G. Ramis, G. Garbarino, A. Di Michele, ChemCatChem, 5 (2013) 294-306.

19. Z. He, M. Yang, X. Wang, Z. Zhao, A. Duan, Catal. Today, 194 (2012) 2-8.

20. S.J. Tauster, S.C. Fung, R.L. Garten, J. Amer. Chem. Soc., 100 (1978) 170-175.

21. S.J. Tauster, Acc. Chem. Res., 20 (1987) 389-394.

22. S. Subramanian, Platinum Metals Rev., 36 (1992) 98-103.

23. V. Nichele, M. Signoretto, F. Menegazzo, A. Gallo, V. Dal Santo, G. Cruciani, G. Cerrato, Appl. Catal. B: Environ., 111-112 (2012) 225-232.

24. Selected Powder Diffraction Data, Miner. DBM, JCPDS, Swarthmore, PA, 1 (1974–1992) 40.

25. S. Brunauer, P.H. Emmett, E. Teller, J. Am. Chem. Soc., 60 (1938) 309-319.

26. E.P. Barrett, L.G. Joyner, P.P. Halenda, J. Am. Chem. Soc., 73 (1951) 373-380.

27. V. Nichele, M. Signoretto, F. Menegazzo, I. Rossetti, G. Cruciani, Int. J. Hydrogen Energy, in press.

28. J.D. Bracey, R. Burch, J. Catal., 86 (1984) 384-391.

29. J. Chen, N. Yao, R. Wang, J. Zhang, Chem. Eng. J., 148 (2009) 164-172.

30. C.D. Dave, K.K. Pant, Renew. Energy, 36 (2011) 3195-3202.

31. M.J. Lazaro, Y. Echegoyen, C. Alegre, I. Suelvea, R. Moliner, J.M. Palacios, Int. J. Hydrogen Energy, 33 (2008) 3320-3329.

32. S. Li, M. Li, C. Zhang, S. Wang, X. Ma, J. Gong, Int. J. Hydrogen Energy, 37 (2012) 2940-2949.

33. S. Li, C. Zhang, Z. Huang, G. Wu, J. Gong, Chem. Commun., 49 (2013) 4226-4228.

34. A.S.P. Lovón, J.J. Lovón-Quintana, G.I. Almerindo, G.P. Valença, M.I.B. Bernardi, V.D. Araújo, T.S. Rodrigues, P.A. Robles-Dutenhefner, H.V. Fajardo, J. Power Sources, 216 (2012) 281-289.

35. D. Zhang, J. Sol-Gel Sci. Technol., 58 (2011) 312-318.

36. P. Guo, L. Guo, in: Detlef Stolten, Thomas Grube (Eds.), 18th World Hydrogen Energy Conference 2010 - WHEC 2010 - Parallel Sessions Book 3: Hydrogen Production Technologies - Part 2, Proceedings of the WHEC, May 16.-21. 2010, Essen - Schriften des Forschungszentrums Jülich / Energy & Environment, 78 (3) (2010) 601-608 - Institute of Energy Research - Fuel Cells (IEF-3) - Forschungszentrum Jülich GmbH, Zentralbibliothek, Verlag.

37. S.D. Sharma, D. Singh, K.K. Saini, C. Kant, V. Sharma, S.C. Jain, C.P. Sharma, Appl. Catal. A: General, 314 (2006) 40-46.

38. L.P.R. Profeti, E.A. Ticianelli, E.M. Assaf, Int. J. Hydrogen Energy, 34 (2009) 5049-5060.

39. L. Chen, C.K.S. Choong, Z. Zhong, L. Huang, Z. Wang, J. Lin, Int. J. Hydrogen Energy, 37 (2012) 16321-16332.

40. M. Domínguez, E. Taboada, E. Molins, J. Llorca, Catal. Today, 193 (2012) 101-106.

41. A.F. Cunha, Y.J. Wu, J.C. Santos, A.E. Rodrigues, Ind. Eng. Chem. Res., 51 (2012) 13132-13143.

42. E. Martono, J.M. Vohs, J. Catal., 291 (2012) 79-86.

43. R.R. Davda, J.W. Shabaker, G.W. Huber, R.D. Cortright, J.A. Dumesic, Appl. Catal. B: Environmental, 56 (2005) 171-186.

44. I.V. Deinega, L.Yu. Dolgykh, I.L. Stolyarchuk, L.A. Staraya, P.E. Strizhak, E.M. Moroz, V.P. Pakharukova, D.A. Zyuzin, Theoretical and Experimental Chemistry, 48 (2013) 386-393.

45. B. Jongsomjit, T. Wongsalee, P. Praserthdam, Catal. Commun., 6 (2005) 705-710.

46. R. Espinal, E. Taboada, E. Molins, R.J. Chimentao, F. Medina, J. Llorca, Appl. Catal. B: Environmental, 127 (2012) 59-67.

47. S. Guerrero, I. Guzmán, G. Aguila, P. Araya, Catal. Commun., 11 (2009) 38-42.

48. J.A. Gadsden, Infrared Spectra of Minerals and Related Inorganic Compounds, Butterworths eds., Reading Mass., USA, 1975.

49. V. Sanchez-Escribano, L. Arrighi, P. Riani, R. Marazza, G. Busca, Langmuir, 22 (2006) 9214-9219.

50. F. Boccuzzi, S. Coluccia, G. Martra, N. Ravasio, J. Catal., 184 (1999) 316-326.

51. R. Kumar, S.R. Dhakate, T. Gupta, P. Saini, B.P. Singh, R.B. Mathur, J. Mater. Chem. A, 1 (2013) 5727.

Table 1: Main physical-chemical properties of the Ni-based samples**.** Ni loading from atomic absorption analysis. SSA = Specific surface area, from BET model. Crystal size determined by Rietveld analysis after reduction at 500 or 800°C according to the calcination temperature; values in parentheses refer to the spent catalyst. H_2/NiO represents H_2 uptake normalised per mol of NiO during TPR analysis.

Sample	**Preparation method**	**Ni (wt%)**	**SSA (m^2/g)**	**Mean pore size (nm)**	**Crystal size (nm)**	**H_2 / NiO (mol/mol)**
T_AC5Ni	TiO_2 prepared by precipitation with NH_3, calcined at 500°C	7.5	100	4.5	7	2.5
T_SC5Ni	TiO_2 prepared by precipitation with NaOH, calcined at 500°C	7.8	101	4.1	7 (44)	2.15
T_AC8Ni	TiO_2 prepared by precipitation with NH_3, calcined at 800°C	7.3	7	32	27	1.05
T_SC8Ni	TiO_2 prepared by precipitation with NaOH, calcined at 800°C	6.7	4	-	27 (27)	1.23

Table 2: Main physical-chemical properties of the samples Co and Cu-based samples.

Sample	Preparation method	Co, Cu (wt%)*	SSA (m^2/g)**	Mean pore size (nm)	Crystal size (nm)***
T_AC5Co	TiO_2 prepared by precipitation with NH_3, calcined at 500°C	6.6	88	6.4	8
T_SC5Co	TiO_2 prepared by precipitation with NaOH, calcined at 500°C	9.6	51	10.1	21
T_AC5Cu	TiO_2 prepared by precipitation with NH_3, calcined at 500°C	5.6	73	8.1	7
T_SC5Cu	TiO_2 prepared by precipitation with NaOH, calcined at 500°C	5.6	49	12.0	10

* From atomic absorption analysis.
** SSA = Specific surface area, from BET model.
*** Crystal size determined by the Scherrer equation

Table 3: Activity for ESR of Ni/TiO_2 catalysts. Reaction temperature 500°C, H_2O/CH_3CH_2OH = 3 (mol/mol); GHSV = 1750 h^{-1}. Productivity defined as H_2 molar flow at reactor outlet per kg of catalyst. Average values between 4-8 h-on-stream.

	Blank	**T_AC5Ni**	**T_SC5Ni**	**T_AC8Ni**	**T_SC8Ni**
C Balance (%)	91 ± 6	80 ± 4	75.3 ± 0.4	70 ± 6	76.7 ± 1.1
H_2 Productivity (mol/min kg_{cat})	0.0	0.0	0.24*	0.91 ± 0.13	0.84 ± 0.02
CO/CO_2	0.0	0.0	0.0	8.7 ± 0.2	1.32 ± 0.14
H_2O Conv. (%)	65 ± 6	72.9 ± 0.9	67 ± 3	51 ± 12	35 ± 9
CH_3CH_2OH Conv. (%)	13 ± 6	26 ± 4	30.9 ± 0.7	89 ± 9	99.5 ± 1.0
CH_3CHO Sel. (%)	24 ± 10	17 ± 4	16.4 ± 1.4	2.7 ± 0.6	0.2 ± 0.3
CH_4 Sel. (%)	0.0	0.0	0.0	9.9 ± 1.0	7.1 ± 0.3
CH_2CH_2 Sel. (%)	0.0	0.0	0.0	6 ± 3	0.0

* For the 1st h-on-stream, only, then negligible concentration.

Table 4: Activity for ESR of Co/TiO_2 and Cu/TiO_2 catalysts. Reaction temperature 500°C, H_2O/CH_3CH_2OH = 3 (mol/mol); GHSV = 1750 h^{-1}. Productivity defined as H_2 molar flow at reactor outlet per kg of catalyst.

	Blank	**T_AC5Co**	**T_SC5Co**	**T_AC5Cu**	**T_SC5Cu**
C Balance (%)	91 ± 6	89 ± 6	89 ± 5	51 ± 26	94 ± 8
H_2 Productivity (mol/min kg_{cat})	0.0	0.20*	0.29 ± 0.17	0.36 ± 0.16	0.16*
CO/CO_2	0.0	0.34 ± 0.09	0.98 ± 0.05	15 ± 6	0.47 ± 0.10
H_2O Conv. (%)	65 ± 6	70 ± 3	65 ± 5	65 ± 3	67 ± 5
CH_3CH_2OH Conv. (%)	13 ± 6	32 ± 13	53 ± 7	1.0	16 ± 6
CH_3CHO Sel. (%)	24 ± 10	56 ± 7	52 ± 4	17 ± 10	71 ± 54
CH_4 Sel. (%)	0.0	1.1*	3.5 ± 0.3	7 ± 2	0.0
CH_2CH_2 Sel. (%)	0.0	0.0	0.0	7 ± 4	0.0

* Value for the 1st h-on-stream, negligible concentration after then.

Figure 1: Catalytic performance at 500°C vs. time-on-stream. (a) C balance for catalysts T_AC8Ni and T_SC8Ni; (b) Etanol conversion and selectivity to selected by-products of sample T_AC8Ni and (c) T_SC8Ni.

(a)

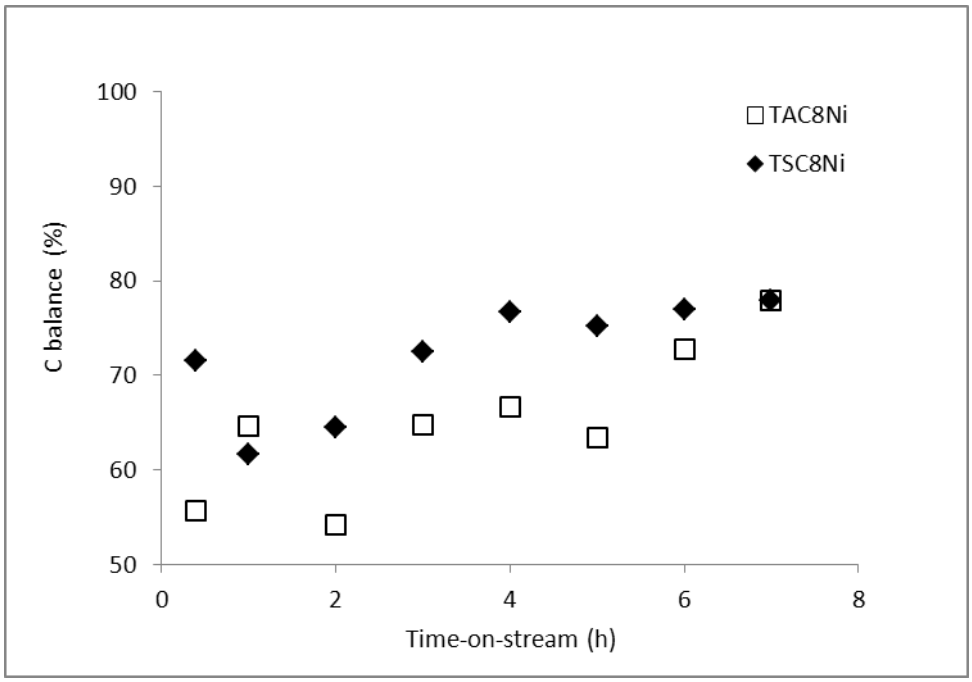

(b)

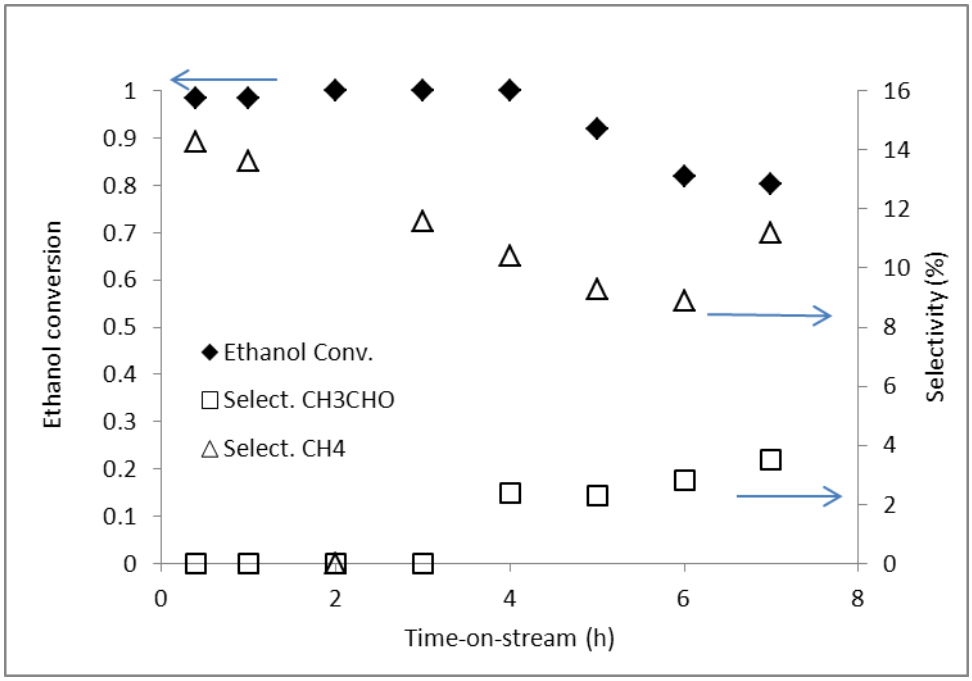

(c)

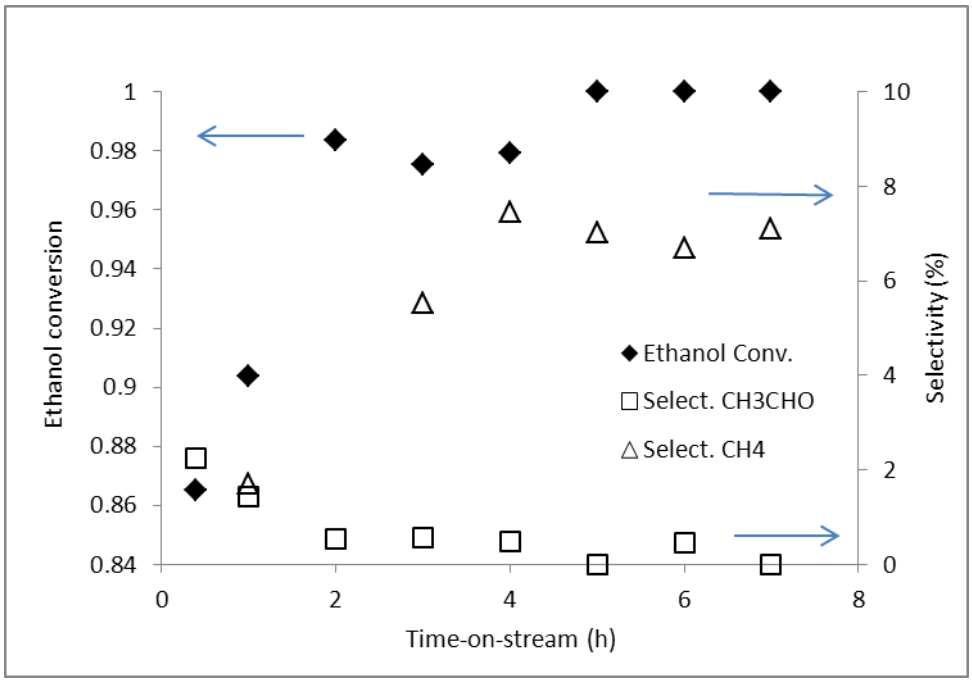

Figure 2: TPR pattern of : (a) Ni/TiO_2 samples ; (b) Co/TiO_2 samples; (c) Cu/TiO_2 samples..

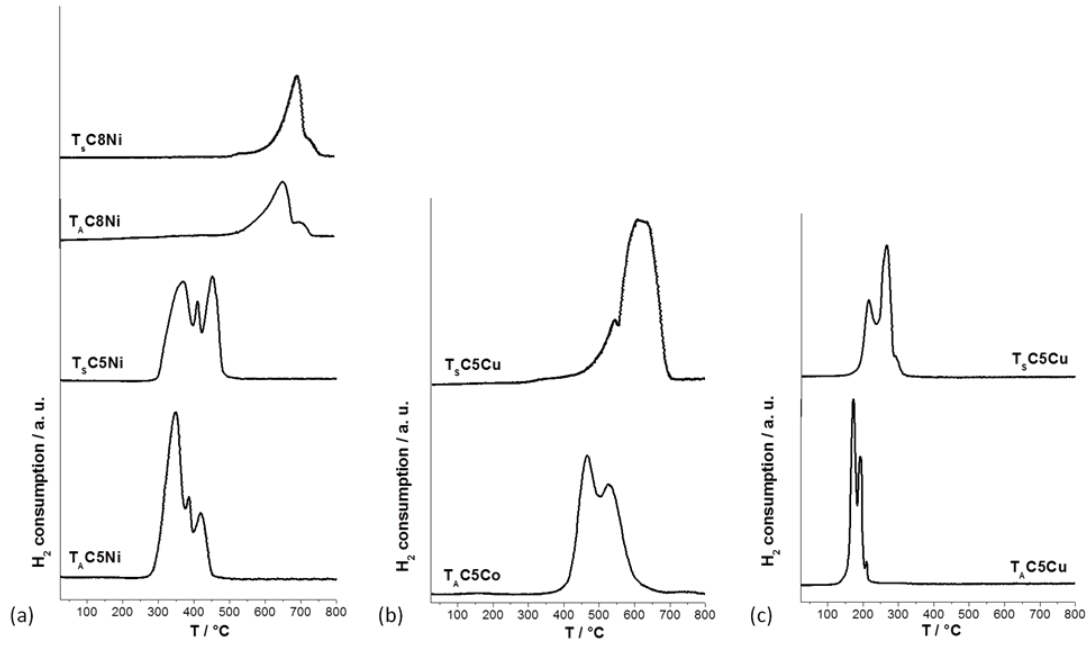

Figure 3: TEM micrographs relative to selected samples after activation for 1 h under 10 vol% H_2/He flow at 500°C for sample T_SC5Ni (a) and 800°C for sample T_SC8Ni (b-d). Marker size 100 nm.

a)

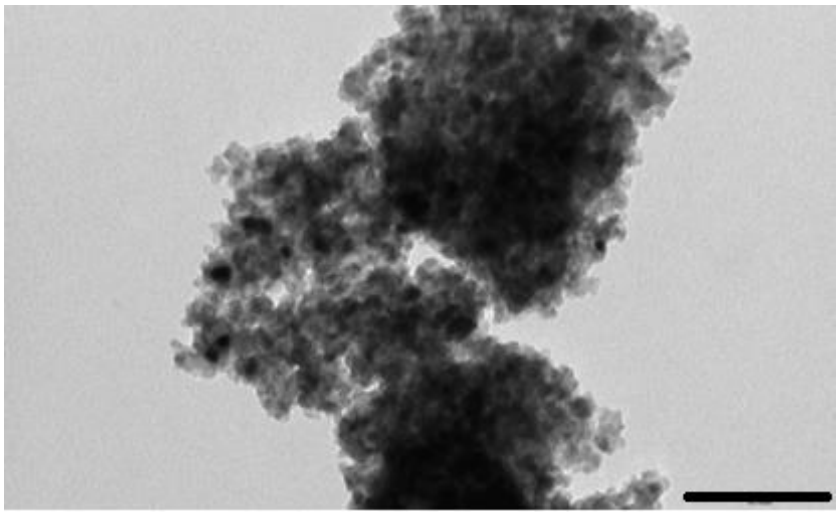

b)

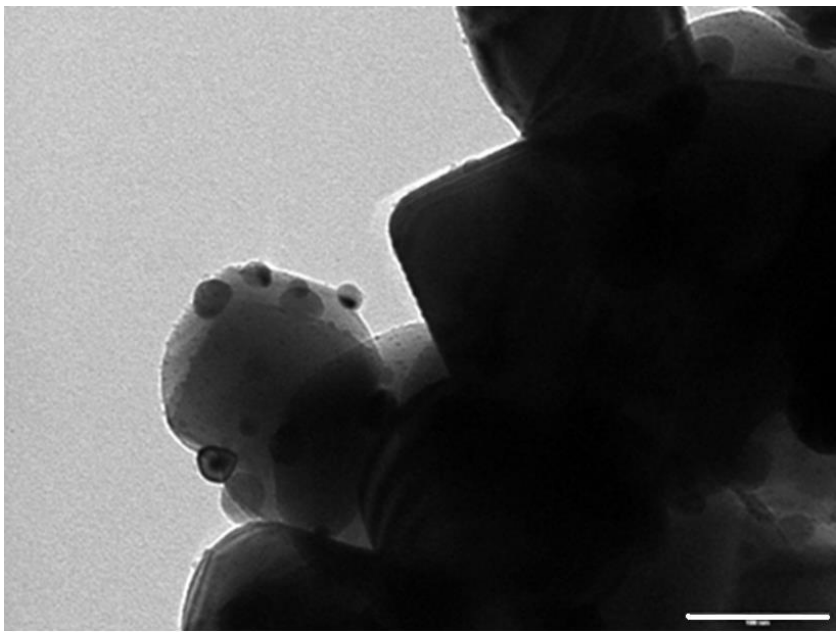

c)

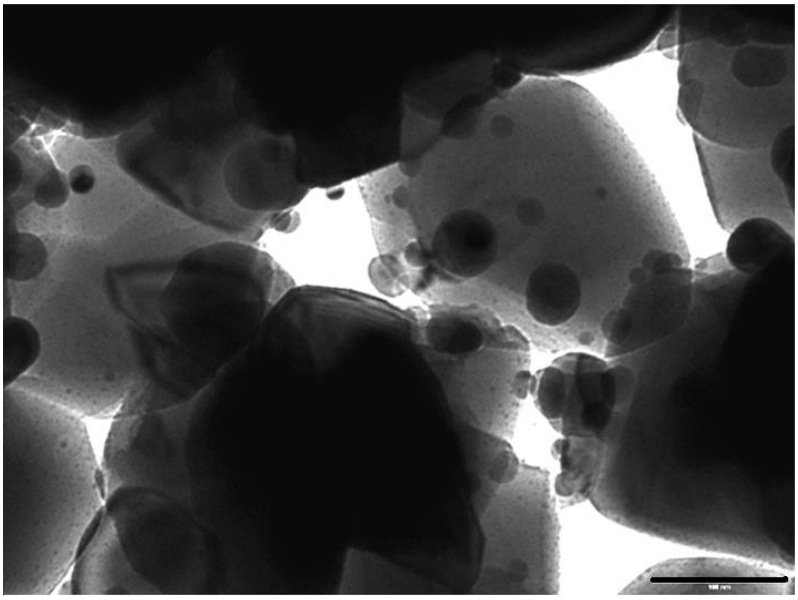

d)

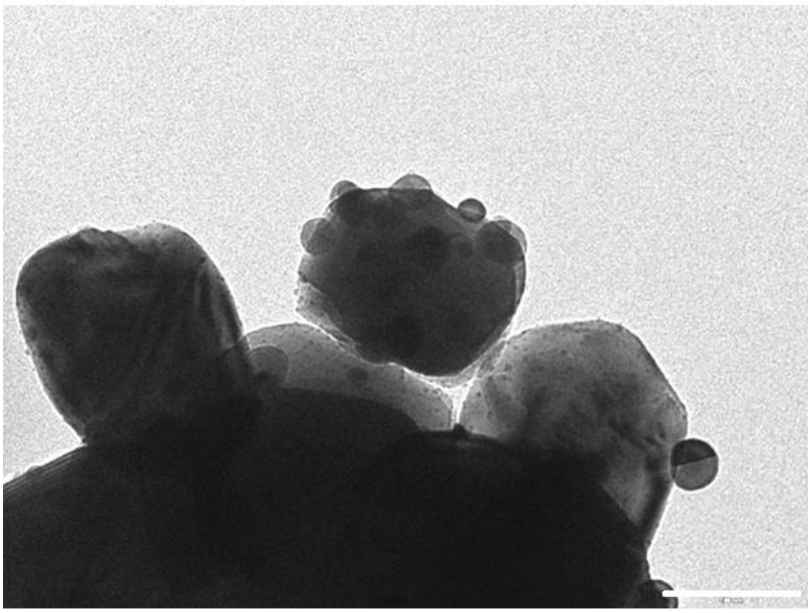

Figure 4. FT IR spectra of surface species arising from low temperature CO adsorption over the T_SC8Ni and T_AC8Ni catalysts. The activated surfaces have been subtracted.

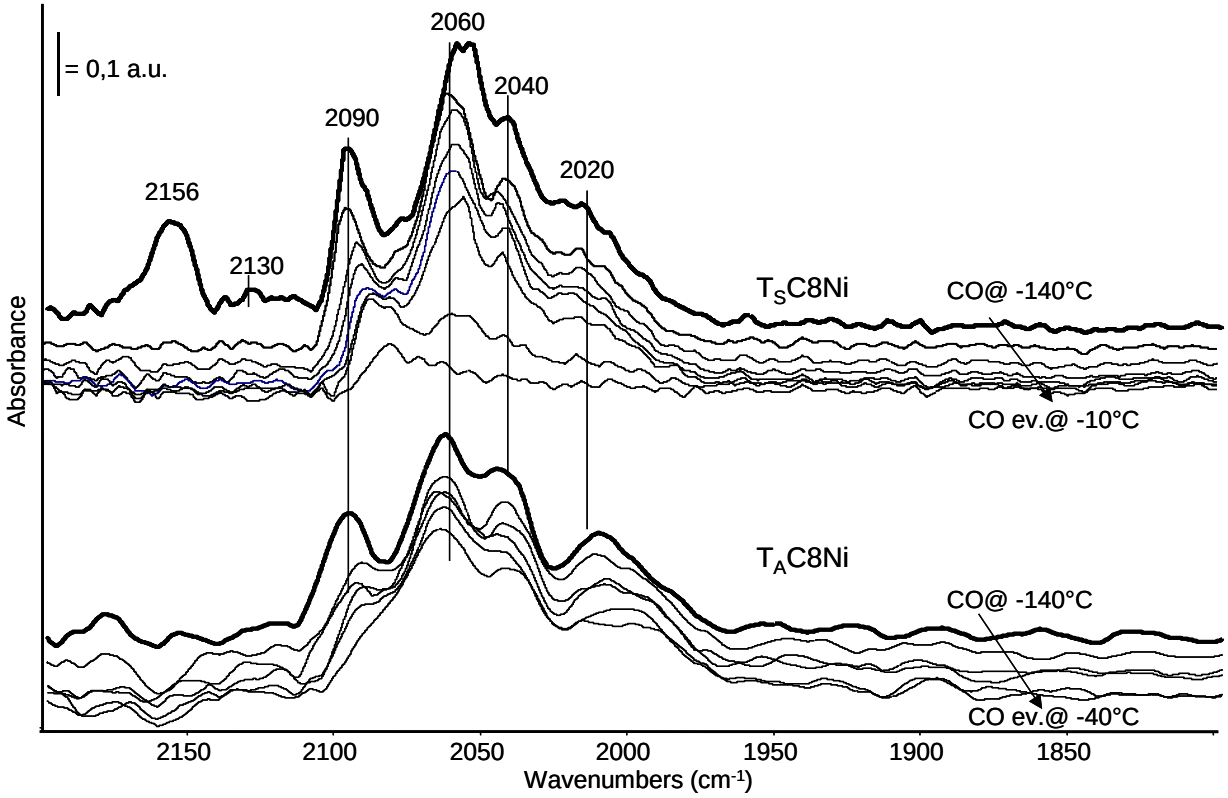

Figure 5. FT IR spectra of surface species arising from low temperature CO adsorption over T_SC5Cu and T_AC5Cu samples reduced in hydrogen at 500°C. The activated surfaces have been subtracted.

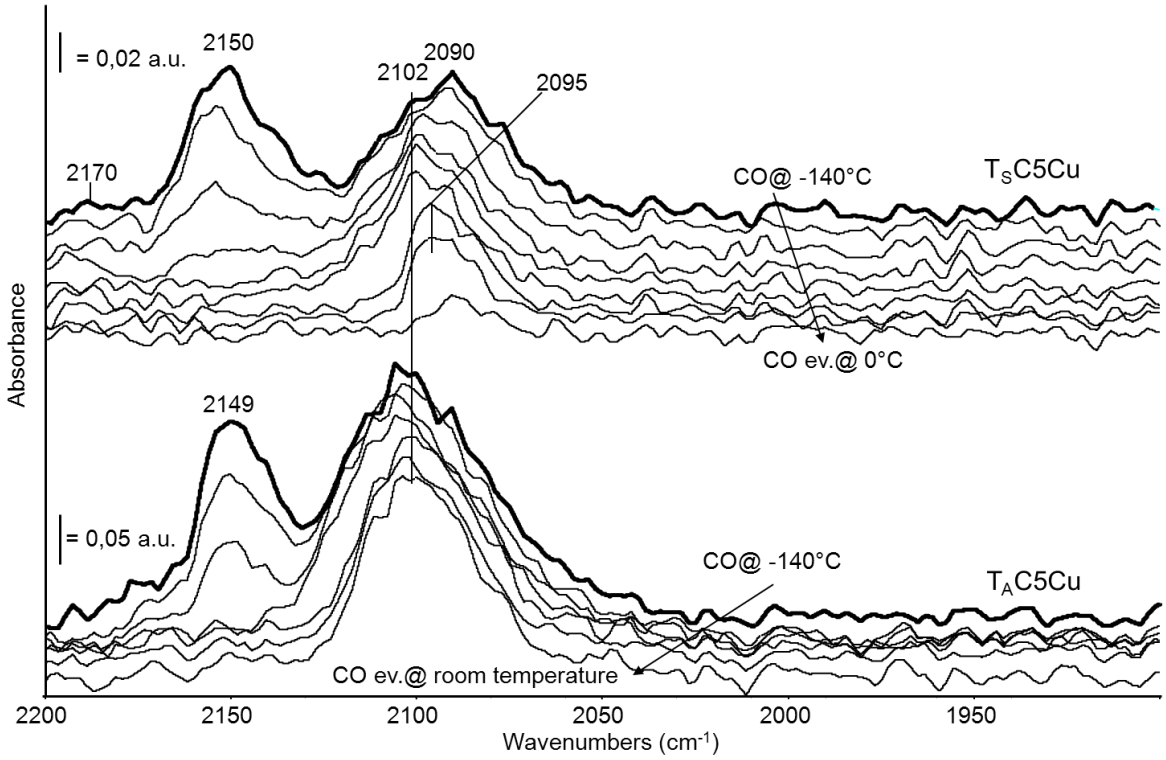

Fig. 6: TEM micrographs of selected spent samples. a) T_SC5Ni; b) T_SC8Ni; c) T_AC5Co; d-e) T_SC5Co; f) T_AC5Cu. Marker size 100 nm.

(a)

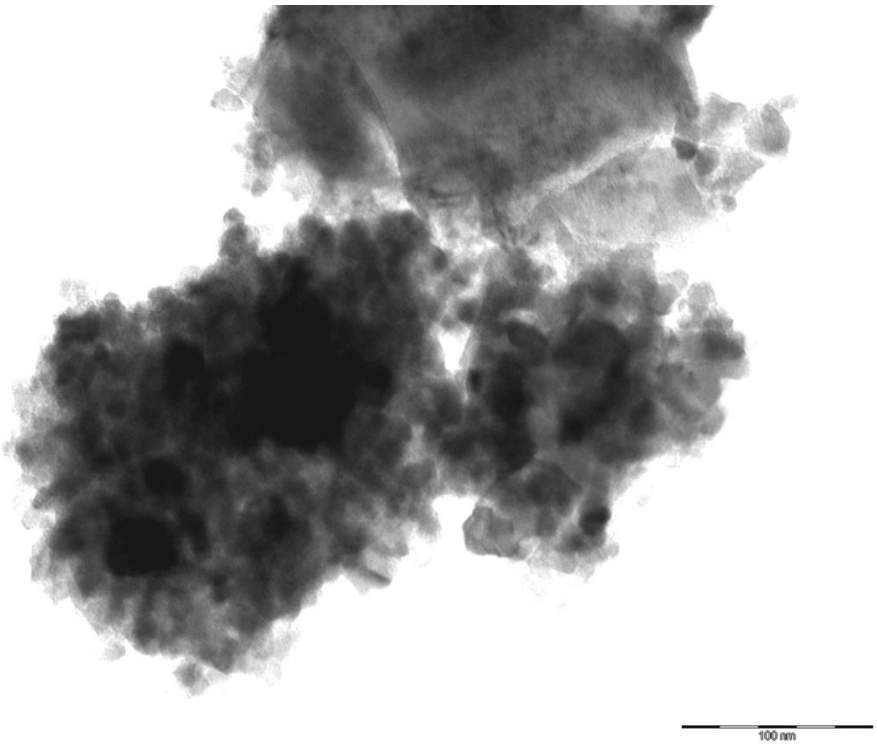

(b)

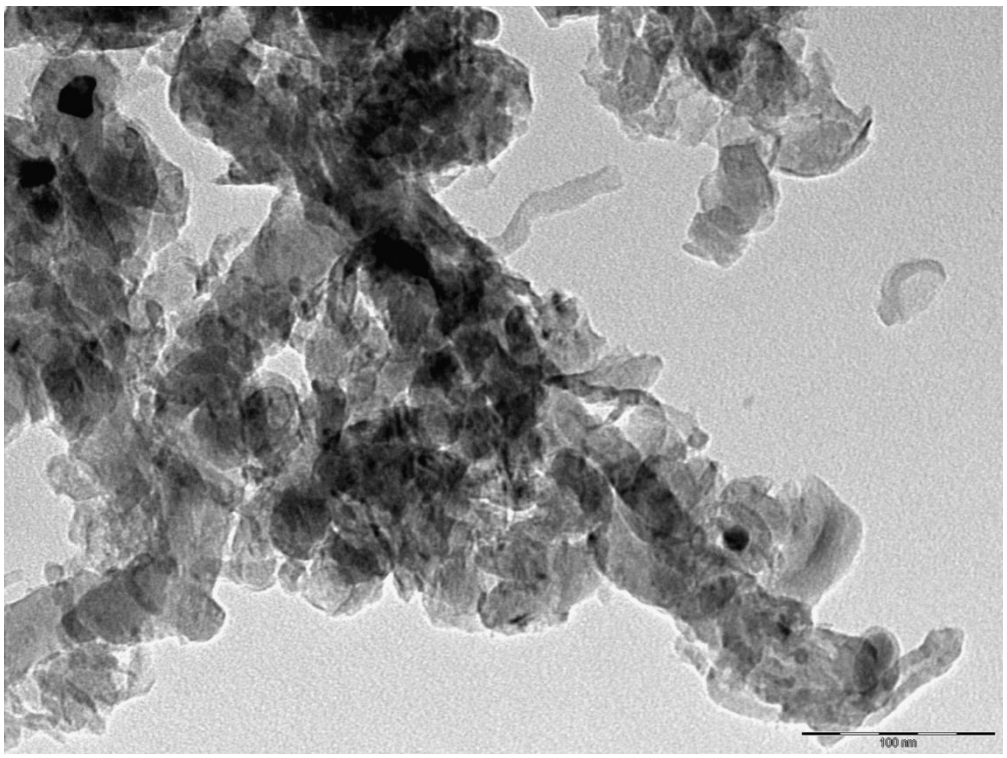

(c)

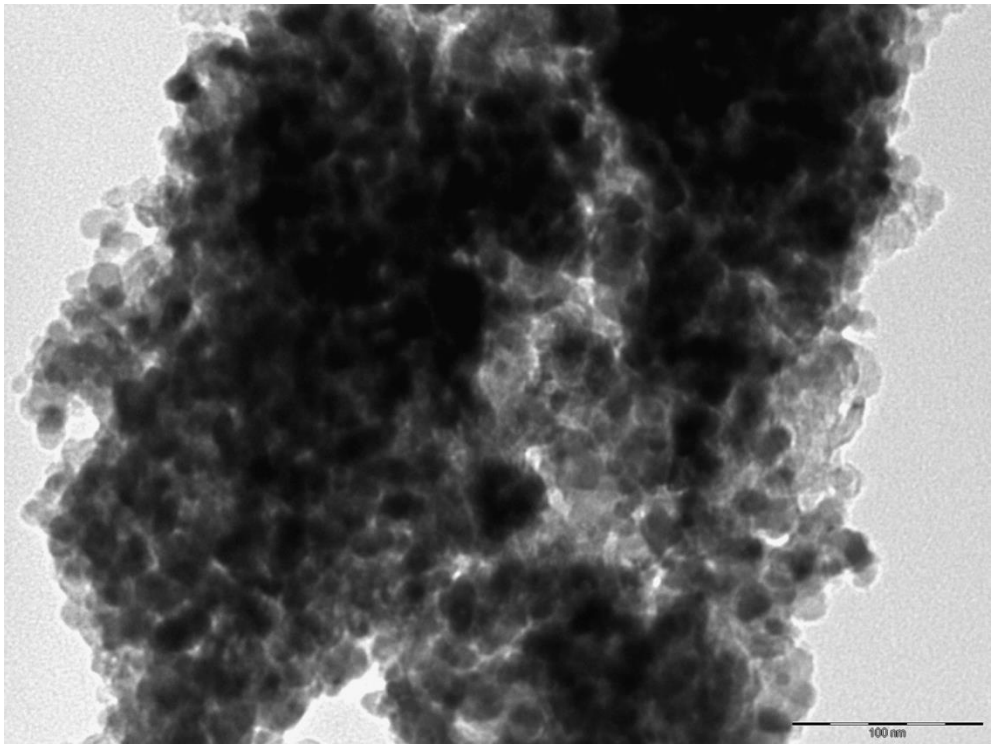

(d)

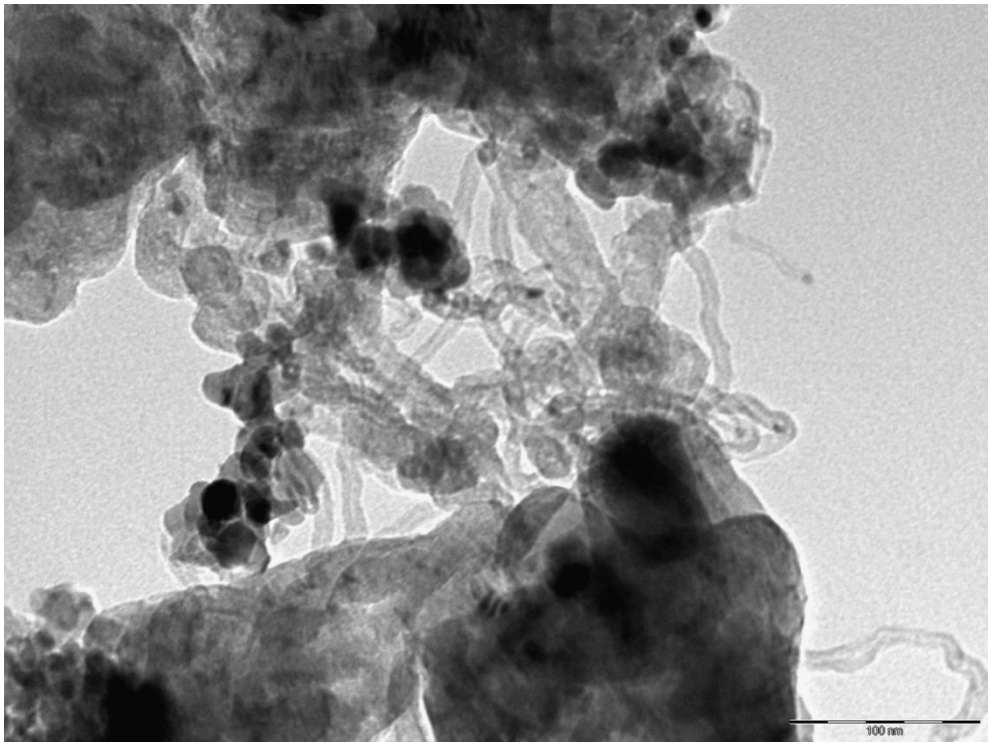

(e)

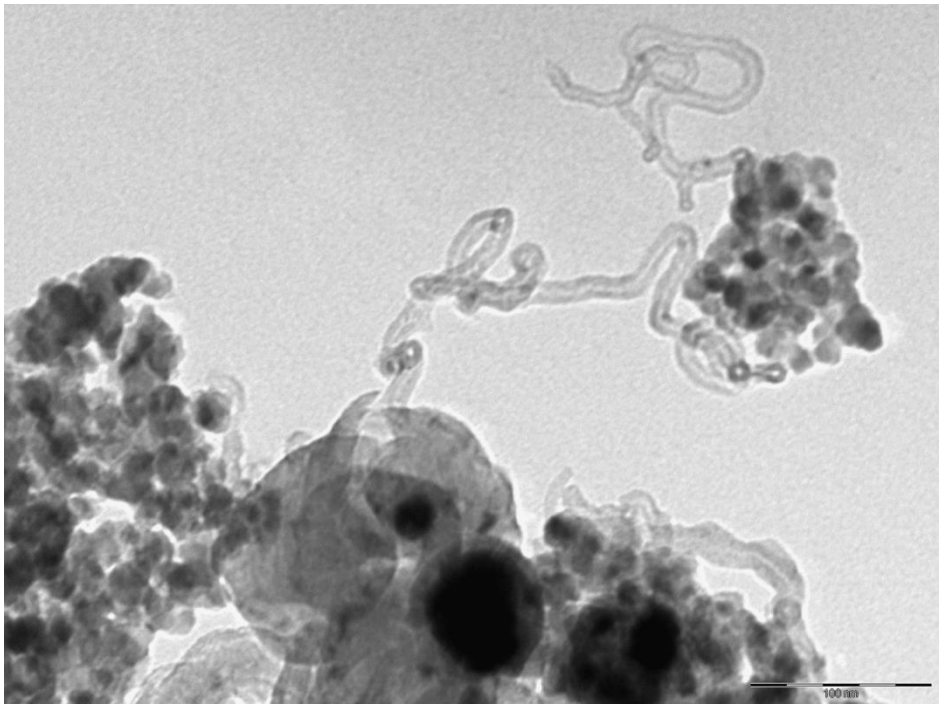

(f)

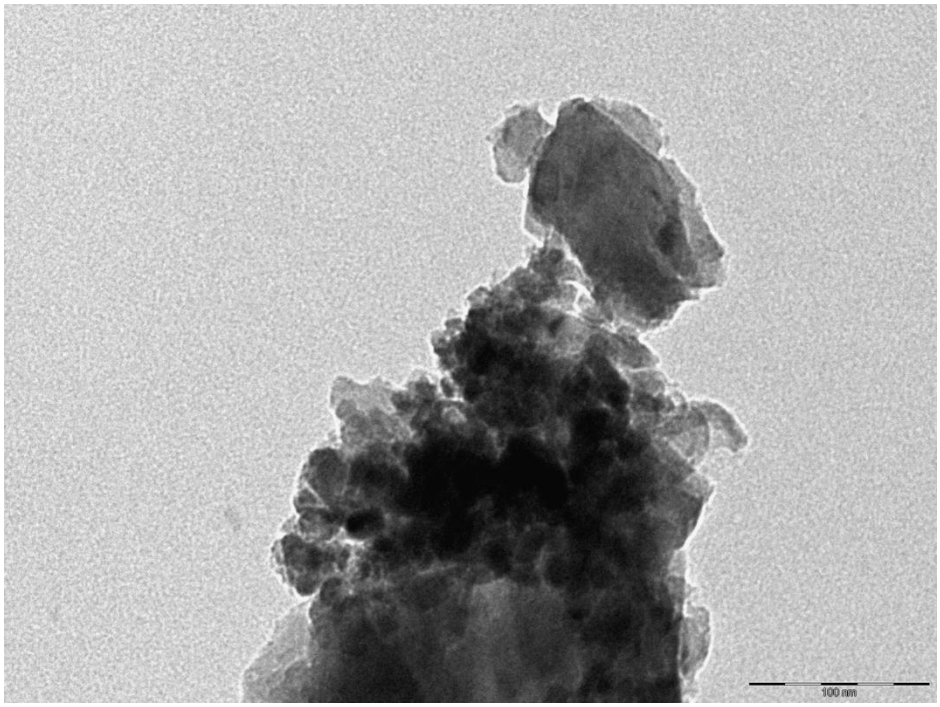

Fig. 7: Raman spectra of spent catalysts.

(a)

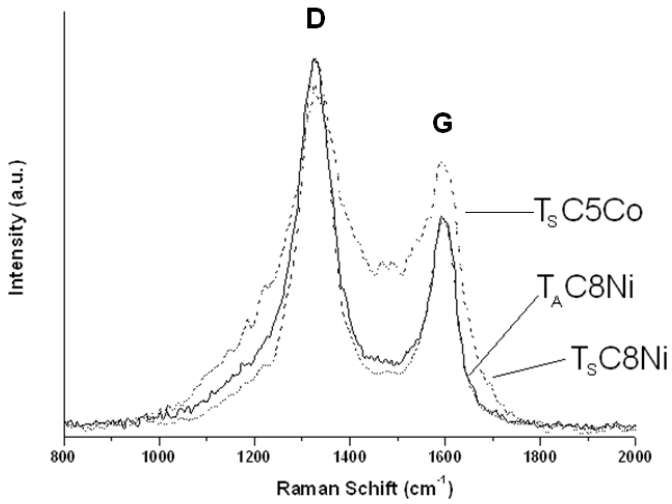

(b)